Dissociative wave packets and dynamic resonances

David Cardoza, Brett J. Pearson, and Thomas Weinacht
Department of Physics, Stony Brook University, Stony Brook, New York 11794

(Received 25 September 2006; accepted 5 January 2007; published online 28 February 2007)

The authors examine the role of dynamic resonances in laser driven molecular fragmentation. The yields of molecular fragments can undergo dramatic changes as an impulsively excited dissociative wave packet passes through a dynamic resonance. The authors compare three different kinds of dynamic resonances in a series of molecular families and highlight the possibility of characterizing the dissociative wave function as it crosses the resonance location. © *2007 American Institute of Physics*. [DOI: 10.1063/1.2437198]

I. INTRODUCTION

There has been an increasing interest in making and measuring wave packets in atomic and molecular systems over the past two decades. Experimental efforts concentrating on bound state wave packets range from Rydberg wave packets in atoms (coherent superpositions of principal quantum number states)[1–3] to rotational,[4–6] vibrational,[7–10] and electronic[11–14] wave packets in molecules. These experiments have observed wave packet oscillations, dephasing, and revivals, and have been applied to problems from quantum computing to ultrafast phase modulation of laser pulses. Dissociative wave packets have also been studied in molecules, making use of femtosecond transition state spectroscopy to follow the dynamics of bond breaking in real time.[15,16] These experiments made use of a dynamic resonance condition in order to follow the evolution of a dissociative wave packet.[17]

Most experiments to date have examined wave packets created in the weak field (perturbative) regime and focused on a particular system. Here we describe a set of nonperturbative experiments that study dissociative vibrational wave packets passing through dynamic resonances in a series of polyatomic ($5 \leqslant n \leqslant 10$) molecules. The emphasis is on comparing different types of dynamic resonances and understanding their role in strong field dissociative ionization.[18] For two of the molecules, we perform wave packet simulations on calculated ionic potential energy surfaces for comparison with measurements. We also discuss how wave packets can be interferometrically measured using dynamic resonances.[19–22] For example, the portion of a dissociative wave packet in the vicinity of a dynamic resonance is transferred to a different state by the probe pulse in a pump-probe measurement. If the wave packet is temporally broader than the laser pulse, the dynamic resonance provides a measure of the instantaneous probability density of the vibrational wave packet as a function of time, and the interference of two wave packets can be used to gain phase information about the wave packet. Furthermore, this information may be used to characterize the dissociative potentials on which the wave packet evolves.[16,23]

As an illustrative example, we consider laser induced dissociation of the model molecule *ABC*. Figure 1 depicts the simplified potential energy surfaces (PESs) involved in the wave packet excitation and subsequent dynamic resonance. An ultrafast "pump" pulse transfers population from PES 1 to PES 2, impulsively launching a dissociative vibrational wave packet on the excited state (e.g., $ABC \rightarrow ABC^{*}$). In the experiments discussed here, PES 2 is ionic, but this is not necessary. As the vibrational wave packet evolves on PES 2, the molecule moves toward dissociation ($ABC^{+} \rightarrow AB^{+}+C$). Since the energy separation between PESs leading to different fragmentation channels will, in general, change with fragment separation, the wave packet may cross a position where a higher lying state (e.g., PES 3) comes into resonance with PES 2. A probe pulse, arriving at the specified time and with the appropriate intensity for a single- (or multi-) photon resonance, will transfer a portion of the wave packet to PES 3. The final state can lead to different charge or fragment distributions than PES 2 (e.g., $AB^{+}+C+nh\nu \rightarrow AB+C^{+}$). Although only three PESs are shown in Fig. 1, we expect that a dissociative wave packet on PES 2 will pass through multiple dynamic resonances with different final

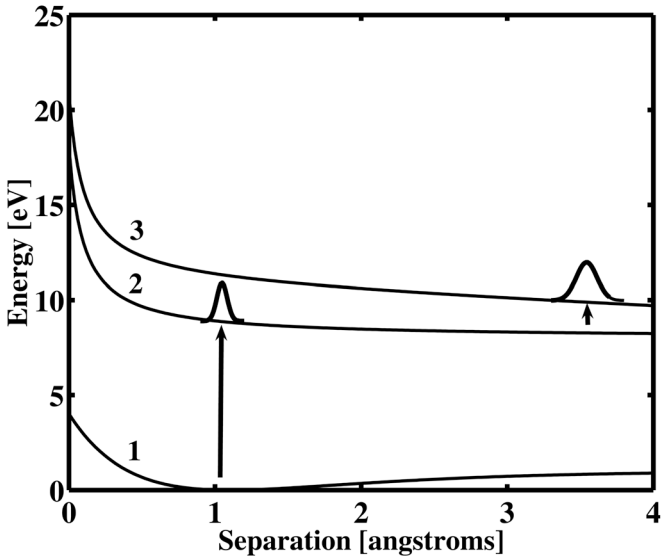

FIG. 1. Model potential energy surfaces describing a dynamic resonance in a dissociating molecule. Population is transferred from the ground state 1 to an excited dissociative state 2. At some point later in time, a second laser pulse promotes the population to state 3.

states. PES 3 represents one of the many possible final electronic states that are accessible from PES 2. In general there will be many different mechanisms for producing multiple fragments ions, and we address this issue after the discussion of the data.

II. EXPERIMENTAL APPARATUS

The experimental apparatus has been described elsewhere.[24] Briefly, we use a titanium:sapphire laser system that produces 30 fs laser pulses with 1 mJ of energy at a repetition rate of 1 kHz. The pulses are directed into a Mach-Zehnder interferometer, where one arm contains an acousto-optic modulator based pulse shaper.[25] The pulse shaper allows control over both the phase and the amplitude of the pump pulses. The other arm of the interferometer acts as a variable delay for a second probe pulse used to probe the dynamics initiated by the pump laser pulse. Both pump and probe laser pulses are focused into an effusive molecular beam, and ions are collected in a time-of-flight mass spectrometer. Peak laser intensities in the interaction region reach the low 10^{14} W/cm^2.

III. DYNAMIC RESONANCES

In previous work on a family of halogenated acetone molecules, we understood the results of a series of molecular fragmentation, learning control experiments in terms of different dynamic resonances.[22,26,27] Here we discuss similarities and differences between different types of dynamic resonances that are distinguishable through measurements of ion fragment yields as a function of pump-probe delay and laser pulse intensity. We discuss two proper resonances, charge transfer ($AB^+ + C + h\nu \rightarrow AB + C^+$) and enhanced dissociation ($AB^+ + C + h\nu \rightarrow A^+ + B + C$), as well as the quasiresonance of enhanced ionization ($AB^+ + C + nh\nu \rightarrow AB^+ + C^+$, $n > 1$).

All three processes involve a dissociative molecular wave packet passing through a fragment separation where the transition probability from an initial PES to a new PES is greatly enhanced. In the cases of enhanced dissociation (ED) and charge transfer (CT), the enhancement is due to a resonant transition (the separation between electronic states is equal to the laser frequency times Planck's constant), whereas in the case of enhanced ionization (EI), the enhancement occurs when the electron tunneling frequency into the continuum becomes roughly equal to and exceeds the laser frequency.

A. Types of dynamic resonances: Charge transfer, enhanced dissociation, and enhanced ionization

We first consider CT and ED dynamic resonances. In the case of CT, both PES 2 and 3 in Fig. 1 are singly charged ionic states, leading to the same product fragments, with the only difference being which fragment retains the charge. The signature of CT is an anticorrelation between the two fragment channels produced on states 2 and 3. ED is similar to CT except that the probe laser transfers the wave packet to a final state (PES 3) that leads to a greater number of fragments.

EI, while technically not a resonance, behaves in a quasiresonant way under the experimental conditions described in this paper. In EI the probability for secondary ionization is enhanced at a particular internuclear separation during dissociation.[28–30] Although the details are more involved, Fig. 1 may still be used to qualitatively represent the process of EI. PES 2 is a singly ionized state of the molecule, while PES 3 is doubly charged. EI is strictly a strong field effect, and we expect PES 3 to be much higher in energy than PES 2, so the arrow depicting the probe coupling in Fig. 1 represents a multiphoton process. As described below, the value of the Keldysh parameter ($\gamma = \omega_{\text{laser}}/\omega_{\text{tunneling}}$, where ω_{laser} is the angular frequency of the laser and $\omega_{\text{tunneling}}$ is the electron tunneling frequency through the external potential barrier into the ionic continuum)[18,31] serves as a method for distinguishing between different types of dynamic resonances.

For single-photon coupling, the resonance condition is defined by $\omega_{\text{laser}} = E_{23}(R)/\hbar$, where R is the interfragment separation and $E_{23}(R)$ is the energy separation between states 2 and 3. When $\gamma > 1$ for all fragment separations R, the peak laser intensity is insufficient to drive efficient EI, and there is little ionization during the probe pulse. However, both charge transfer and enhanced dissociation may occur during dissociation if higher lying PESs come into resonance. If $\gamma \leqslant 1$ for some value of R, the laser intensity is sufficient to drive EI efficiently, and the quasiresonance becomes determined by the laser frequency and tunneling rate(s) of the subsequently removed electron(s). Specifically, after initial ionization by the pump pulse, the fragments begin to separate. During separation $\omega_{\text{tunneling}}(R)$ can increase drastically (by several orders of magnitude) with increasing R, eventually matching the laser frequency at a critical separation R_0. Once the tunneling frequency is equal to or greater than the laser frequency, ionization can proceed rapidly within a fraction of the pulse duration. While the condition for EI is not a strict resonance, EI displays a very similar behavior to CT and ED with higher laser intensities required. We therefore treat EI as a quasiresonance. It should be noted that one must have electron localization on one of the molecular fragments for enhanced ionization to occur.[32] This localization can occur dynamically as the laser frequency matches the tunneling frequency between the Coulomb-type wells around each fragment. However, this is not necessary, and in the cases discussed in this paper (e.g., asymmetric molecules), one of the dissociating fragments is more likely to retain the charge, thereby automatically ensuring electron localization.

B. Pump-probe data and wave packet simulations

In this section we show pump-probe data for members of different molecular families and interpret the results in terms of dynamic resonances. For those molecules where calculated PESs are available, we also compare the experimental data to molecular wave packet simulations.

Figure 2 shows fragment ion signals as a function of pump-probe delay in the molecules $CH_2BrCOCF_3$ (3-bromo-1,1,1-trifluoroacetone, "BrTFA") [panel (a)] and $CHBr_2COCF_3$ (dibromo-1,1,1-trifluoroacetone, "Br_2TFA") [panel (b)]. The data were taken with a strong pump pulse

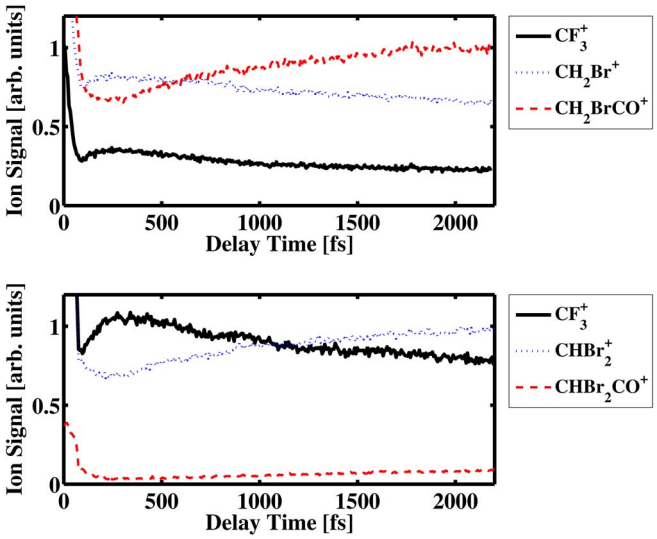

FIG. 2. Fragment ion yields as a function pump-probe delay in $CH_2BrCOCF_3$ (top) and $CHBr_2COCF_3$ (bottom). Each plot shows the primary fragments during the charge-transfer dynamic resonance. All curves for a given molecule are scaled by the same factor. The pump pulse intensity was $\sim 2\times 10^{14}$ W/cm^2, while the probe pulse was approximately one order of magnitude lower.

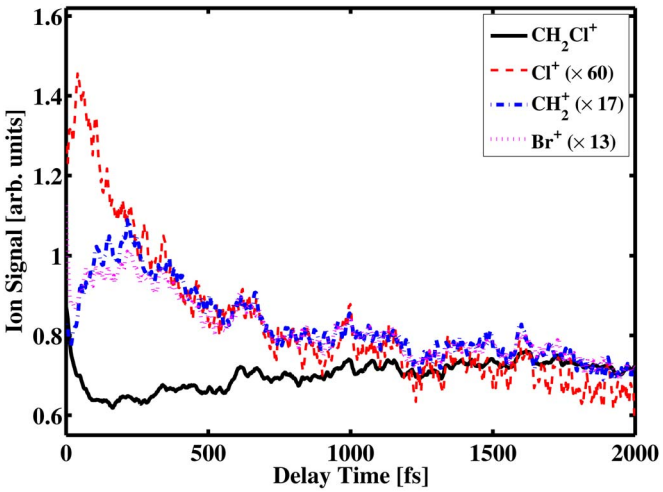

FIG. 3. Fragment ion yields as a function pump-probe delay in CH_2BrCl, showing the primary fragments. The curves are scaled as indicated in the legend. The pump pulse intensity was $\sim 2\times 10^{14}$ W/cm^2, while the probe pulse was approximately one order of magnitude lower.

capable of ionizing the molecule ($\sim 2\times 10^{14}$ W/cm^2) and a relatively weak probe pulse producing no independent ion signal ($<3\times 10^{13}$ W/cm^2). In both molecules, the data show two fragments that are anticorrelated as a function of pump-probe delay, where the widths of the modulations approach 1 ps. The data are consistent with our model of charge transfer developed in Br_2TFA.[22] Specifically, in $CHBr_2COCF_3$, the probe pulse couples the ground ionic state (leading to $CHBr_2^+$ and CF_3) to an excited, charge-transfer state (leading to $CHBr_2$ and CF_3^+). The $CHBr_2^+$ and CF_3^+ yields are anticorrelated, and the increase in one is nearly balanced by the decrease in the other. We note the large degree of modulation (20%–30%) in the yields, indicating a strong coupling between the two PESs. The changes in the $CHBr_2CO^+$ yield are distinct from $CHBr_2^+$, indicating that a separate dynamic resonance leads to the production of this fragment. However, the changes in $CHBr_2CO^+$ are much smaller than the other fragments, so we focus on $CHBr_2^+$ and CF_3^+ here.

It is interesting to note the differences in the BrTFA data. Here CH_2BrCO^+ and CF_3^+ are the fragments that show the largest degree of anticorrelation. These two fragments arise from a single bond breaking (the $C-CF_3$ bond). Furthermore, the yields of these two fragments are no longer balanced. The removal of one Br atom in the composition of the molecule changes the electronic structure of the ion sufficiently to change which states pass through resonance with the probe laser during dissociation. The yield imbalance between CH_2BrCO^+ and CF_3^+ suggests that, in addition to CT, ED is also playing an important role in the dynamics. The increase of the CH_2Br^+ yield, also anticorrelated with CH_2BrCO^+, further supports this idea. In fact, the decrease in CH_2BrCO^+ is balanced by the sum of the CF_3^+ and CH_2Br^+ increases, indicating that the CT and ED resonances discussed here dominate the dissociation dynamics.

Figure 3 shows an example of another molecular family where both CT and ED occur. It plots ion fragment yields as a function of pump-probe delay for the halogenated methane CH_2BrCl (bromochloromethane). Pulse intensities are similar to those used in Fig. 2, and the resonances are again at the single-photon level. In CH_2BrCl, the CH_2Cl^+ fragment is suppressed, while the primary remaining fragments (Br^+, CH_2^+, and Cl^+) are enhanced. We again interpret these data using Fig. 1, where the pump pulse transfers a wave packet from PES 1 to PES 2, leading to CH_2Cl^+. The probe pulse couples the wave packet to multiple higher PESs. The correlated increase in the Br^+ fragment is due to CT, while ED resonances lead to the increases in CH_2^+ and Cl^+. Note that the increase in the Cl^+ yield is not well correlated with the increases in Br^+ and CH_2^+, but occurs earlier in the pump-probe scan. This indicates that the resonance leading to Cl^+ occurs at much smaller CH_2Cl^+-Br distances than the other two resonances (which occur at the same time within the resolution of our measurement). We also note that the sum of all fragment yields is constant to within the experimental noise for all pump-probe delays, implying that the three resonances discussed here account for all of the fragment yield modulations.

Pump-probe data depicting an EI dynamic resonance are shown in Fig. 4. The data are from the halogenated acetone family members 1-trifluoroacetone (CH_3COCF_3, "TFA") [panel (a)] and trichloroacetone (CH_3COCCl_3, "TCA") [panel (b)]. In contrast with the previous results, the data were taken using an intense probe pulse (between 0.5 and 1 times the pump pulse intensity). For lower probe pulse intensities we did not observe any changes in the fragment yields. The most important feature to note in Fig. 4 is that, unlike the previous three molecules, only a single fragment shows any dependence on pump-probe delay (CF_3^+ for TFA and CCl_3^+ for TCA). For comparison, the CH_3^+ signal is also shown. In both molecules, the yield of one charged fragment increases and then decreases as the dissociative wave packet travels through the EI location toward large fragment separations. Although TFA and TCA are similar in this respect,

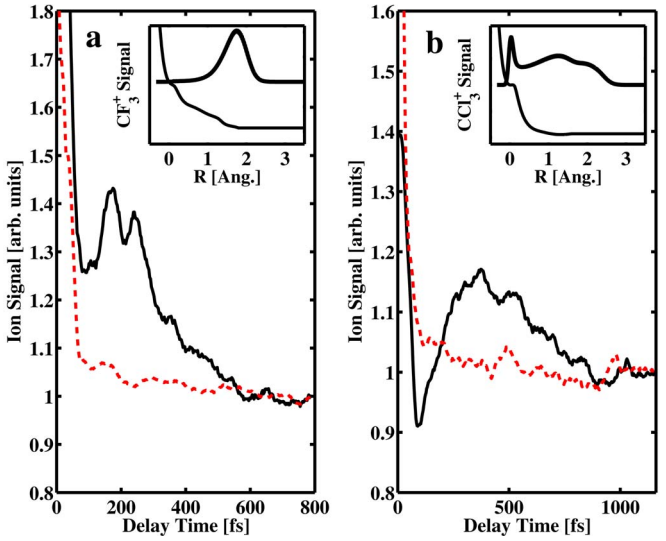

FIG. 4. Fragment ion yields as a function pump-probe delay in CH_3COCF_3 (a) and CH_3COCCl_3 (b). Enhanced ionization is seen in the CF_3^+ (a) and CCl_3^+ (b) fragments (black, solid line). The red, dotted lines plot the CH_3^+ fragment for comparison. Note the different time axes for the two molecules. All curves are individually normalized. The pump pulse intensity was $\sim 4\times 10^{14}$ W/cm^2, while the probe pulse was 0.5–1 times lower. Wave packet simulations on calculated PESs for both molecules are included as insets.

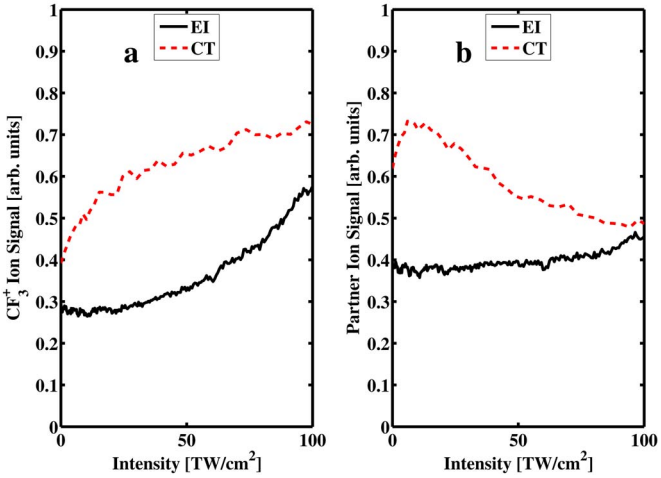

FIG. 5. Ion yield as a function of probe pulse peak intensity for the dynamic resonances of charge transfer (in Br_2TFA) and enhanced ionization (in TFA). Panel (a) plots CF_3^+ for both CT and EI, while panel (b) plots the partner fragment ($CHBr_2^+$ for CT and CH_3^+ for EI). Both curves for each molecule are scaled by the same factor.

the data in TCA suggest a much broader wave packet that arrives at the resonance location later in time than in TFA.

To confirm the interpretation that differences in pump-probe data for the two molecules are a result of wave packet dynamics on the dissociative PES, we performed a series of wave packet calculations on PESs derived from *ab initio* molecular structure calculations. While earlier work[27] demonstrated that a two-dimensional model (including the C–C–O bond angle and C–CF_3 bond length) provides a good description of the dissociation dynamics, wave packet calculations on one-dimensional curves adequately capture many of the qualitative differences between TCA and TFA. For simplicity, we therefore limit ourselves to calculations on one-dimensional PESs of the ionic ground state in TCA and TFA.

Both experimental data and calculations indicate that the molecular ion breaks up into CX_3 (X=F,Cl) and CH_3CO^+ following ionization.[26] As the dissociative wave packet moves towards larger R, it passes through the resonance location where the CX_3 fragment is efficiently ionized by the probe laser field. The insets of Figs. 4(a) (TFA) and 4(b) (TCA) show the calculated dissociative wave packet on the one-dimensional ionic PES as the leading edge passes through the enhanced ionization point R_0. In the simulations, the initial wave packet is determined by projecting the neutral ground state wave function onto the ionic state. The calculations confirm the experimental observation that in comparison to TFA, the wave packet in TCA moves more slowly and spreads more before reaching the resonance location. This is because the ionic PES in TCA has a smaller slope (by a factor of 3) near the initial separation, giving the wave packet a slow start and allowing it to spread more as it moves toward dissociation. The double peaked feature in the experimental TFA pump-probe data can be explained by taking into account the more complete two-dimensional PES,[27] which we do not consider here for simplicity.

C. Intensity scaling and generality of dynamic resonances

As discussed in Sec. III A, depending on the properties of both the molecular system (energy level separations) and the laser pulse (peak intensity of the field), different types of dynamic resonances occur en route to dissociation. We expect lower-order dynamic resonances such as CT to occur when the photon energy of the probe laser (or low multiples thereof) comes into resonance with the separation of two electronic states at some finite fragment distance. This condition is satisfied in Br_2TFA, BrTFA, and CH_2BrCl. If this condition is not met (e.g., in TFA and TCA), a tunneling dynamic resonance such as EI can still occur as the molecular fragments dissociate. There is every indication that EI is general and should occur whenever dynamic (or static) localization of the electronic wave function occurs and pulse intensities are sufficient to drive tunnel ionization at some point during dissociation.[19]

Because EI is a multiphoton process and CT and ED are single-photon events, we characterized the intensity scaling for the different dynamic resonances. Figure 5 shows the dependence of both CT and EI on the peak intensity of a probe pulse centered at the resonance time after the pump. In Fig. 5 the y intercepts are nonzero since the pump pulse creates an ion signal for all fragments independent of the probe pulse. Panel (a) shows the CF_3^+ signal for CT in Br_2TFA (dashed) and EI in TFA (solid). In CT, the CF_3^+ product fragment shows an initial linear increase with intensity, after which point it begins to roll over. In contrast, during EI the CF_3^+ fragment strongly resembles typical multiphoton intensity scaling, where fragment signals increase with a large (>3) multiphoton order.[33]

Panel (b) shows the partner fragments for both cases: $CHBr_2^+$ for CT and CH_3^+ for EI. In CT, the partner fragment

shows a corresponding decrease with increasing probe pulse intensity as the probe pulse drives the CT process. In EI, the partner fragment stays relatively constant as the probe intensity is increased. Once the probe pulse reaches an intensity sufficient to drive ionization independent of the pump pulse, CH_3^+ begins to increase.

As noted earlier, subtle changes within a molecular family (e.g., exchanging one or two atoms for another from the same column of the periodic table) can affect the number and type of dynamic resonances that occur. As an example of the interplay between lower-order and higher-order dynamic resonances, we examined another member of the halogenated acetone family, CCl_3COCF_3 (1,1,1-trichloro-3,3,3-trifluoroacetone, "TFA-TCA"). Through addition of complementary halogen atoms to the other side of TFA, TFA-TCA showed a strong anticorrelation between the CF_3^+ and CCl_3^+ fragments in a pump-probe scan, indicating a CT dynamic resonance where the electron is transferred from CF_3 to CCl_3^+. The data are similar to BrTFA and Br_2TFA (see Fig. 2) and are consistent with the idea that the electronegativity balance between the two sides of the molecule plays a role in dynamic resonances, with an imbalance in electronegativity favoring EI.

A natural question regarding fragmentation is which PESs lead to the formation of specific fragments. That is, can one associate each fragment with a unique PES? We consider three distinct possibilities that may contribute to the fragment yields. One is that a given PES leads to one of the measured fragments with near 100% probability. Another is that a given PES leads to multiple fragments, with the yields being proportional to the branching ratio of the fragments on the PES. A final possibility is that a given PES leads to a single fragment with near 100% branching ratio (such as in the first scenario), but during dissociation the PES encounters level crossings where other PESs come into (near) degeneracy.[34] In this case the fragment yields are affected by the probabilities for traversing these level crossings either adiabatically or diabatically.

To distinguish between these possibilities, we measured fragment ion yields as a function of laser intensity for a single pump pulse. We expect that the pulse intensity should not affect the likelihood of curve crossings if the crossing occurs after the pulse is off. Given the duration of our laser pulse (30 fs), the probability of a curve crossing occurring during the pulse duration is small. Furthermore, we expect that any strong field deformation of the PES on which the wave packet is born will have no effect on the momentum of the wave packet, as there is negligible wave packet movement during the duration of the pulse. Similarly, we expect that the pulse intensity should not affect the branching ratios for a given PES since the pulse duration is so much shorter than the propagation time on the excited state. Therefore, we argue that if the relative ion yields of two different fragments vary with intensity, then the two fragments originate from different PESs.

Figure 6 plots the yields of the three relevant fragment ions from Br_2TFA as a function of intensity for a single pump pulse. The yields are shown as a percentage of the total ion yield of all prominent fragments. We note that $CHBr_2^+$ and $CHBr_2CO^+$ display similar behavior as the intensity is decreased towards zero (at very low intensities the noise increases as the total ion yield approaches zero). Using our current information, we are unable to determine whether the $CHBr_2^+$ and $CHBr_2CO^+$ fragments result from the same PES with a definite branching ratio (approximately 3:1 at low intensities), from two similar but separate PESs, or from two PESs that meet in a curve crossing en route to dissociation. However, the CF_3^+ fragment displays very different intensity scaling, suggesting that it originates from a separate PES, consistent with the assumptions above. Thus, we conclude that CT in Br_2TFA takes place between two different PESs.

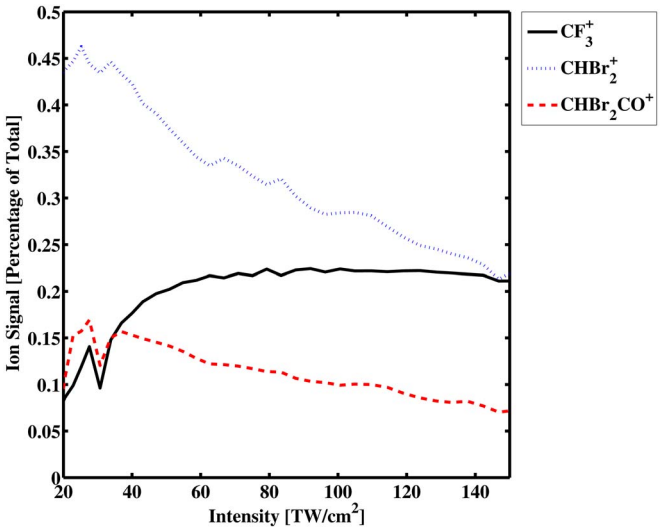

FIG. 6. Fractional ion yield as a function of pump pulse peak intensity in Br_2TFA. The three relevant fragment yields are plotted as a percentage of the total ion yield of all prominent fragments. Below 25 TW/cm^2 the total yield drops quickly to zero, and noise begins to dominate.

IV. CONCLUSIONS

We have described and shown how different types of dynamic resonances influence the behavior of large molecules in short laser pulses. We have identified three general categories of dynamic resonances including charge transfer, enhanced dissociation, and enhanced ionization. All three are characterized by molecular excitation that it is sensitive to interfragment separations as the molecule dissociates. We expect these resonance to be quite general in large, polyatomic molecules.[35–37]

In addition to playing an important role in laser driven molecular fragmentation, dynamic resonances can serve as a window for viewing dissociative wave packets. By adding a secondary pump pulse to the experiments described above, one creates two wave packets that interfere on the dissociative state. Measuring the probability density of the total wave packet as it passes through the dynamic resonance permits access to the phase information contained in the wave function. We have made preliminary measurements that show promise for characterizing both the amplitude and the phase of a dissociating wave packet. However, there are significant experimental hurdles that make this type of measurement challenging, including optical interference and an entanglement-driven damping of the constructive molecular

interference associated with the electronic degree of freedom. By generalizing the experiments to include multiple pump and probe wavelengths, as well as using shorter duration probe pulses from a recently constructed continuum generation source, we hope to improve our ability to measure dissociating wave functions and make use of dynamic resonances in further control experiments.

ACKNOWLEDGMENTS

The authors gratefully acknowledge Steffi Gräfe for helpful discussions during the preparation of the paper. This research was supported by the National Science Foundation (Award No. 0555214).

[1] J. A. Yeazell, M. Mallalieu, J. Parker, and J. C. R. Stroud, Phys. Rev. A **40**, 5040 (1989).
[2] L. D. Noordam and R. R. Jones, J. Mod. Opt. **44**, 2515 (1997).
[3] T. C. Weinacht, J. Ahn, and P. H. Bucksbaum, Phys. Rev. Lett. **80**, 5508 (1998).
[4] P. M. Felker, J. S. Baskin, and A. H. Zewail, J. Phys. Chem. **90**, 724 (1986).
[5] T. Seideman, J. Chem. Phys. **103**, 7887 (1995).
[6] R. Uberna, Z. Amitay, R. A. Loomis, and S. R. Leone, Faraday Discuss. **113**, 385 (1999).
[7] M. J. J. Vrakking, D. M. Villeneuve, and A. Stolow, Phys. Rev. A **54**, R37 (1996).
[8] C. Leichtle, W. P. Schleich, I. S. Averbukh, and M. Shapiro, Phys. Rev. Lett. **80**, 1418 (1999).
[9] D. Zhong and A. H. Zewail, J. Phys. Chem. A **102**, 4031 (1998).
[10] A. Zucchetti, W. Vogel, D.-G. Welsch, and I. A. Walmsley, Phys. Rev. A **60**, 2716 (1999).
[11] H. H. Fielding, J. Phys. B **27**, 5883 (1994).
[12] F. Texier and C. Jungen, Phys. Rev. Lett. **81**, 4329 (1998).
[13] J. Itatani, J. Levesque, D. Zeidler, H. Niikura, H. Pépin, J. C. Kieffer, P. B. Corkum, and D. M. Villeneuve, Nature (London) **432**, 867 (2004).
[14] M. Amano and K. Takatsuka, J. Chem. Phys. **122**, 084113 (2005).
[15] M. J. Rosker, M. Dantus, and A. H. Zewail, J. Chem. Phys. **89**, 6113 (1988).
[16] M. Dantus, M. J. Rosker, and A. H. Zewail, J. Chem. Phys. **89**, 6128 (1988).
[17] M. Lein, M. Erdmann, and V. Engel, J. Chem. Phys. **113**, 3609 (2000).
[18] R. J. Levis and M. J. DeWitt, J. Phys. Chem. A **103**, 6493 (1999).
[19] T. Seideman, M. Y. Ivanov, and P. B. Corkum, Chem. Phys. Lett. **252**, 181 (1996).
[20] E. Skovsen, M. Machholm, T. Ejdrup, J. Thøgersen, and H. Stapelfeldt, Phys. Rev. Lett. **89**, 133004 (2002).
[21] S. Gräfe, D. Scheidel, V. Engel, N. E. Henriksen, and K. B. Møller, J. Phys. Chem. A **108**, 8954 (2004).
[22] D. Cardoza, B. J. Pearson, M. Baertschy, and T. Weinacht, J. Photochem. Photobiol., A **180**, 277 (2006).
[23] R. B. Bernstein and A. H. Zewail, J. Chem. Phys. **90**, 829 (1989).
[24] F. Langhojer, D. Cardoza, M. Baertschy, and T. Weinacht, J. Chem. Phys. **122**, 014102 (2005).
[25] M. A. Dugan, J. X. Tull, and W. S. Warren, J. Opt. Soc. Am. B **14**, 2348 (1997).
[26] D. Cardoza, M. Baertschy, and T. Weinacht, Chem. Phys. Lett. **411**, 311 (2005).
[27] D. Cardoza, M. Baertschy, and T. Weinacht, J. Chem. Phys. **123**, 074315 (2005).
[28] M. Ivanov, T. Seideman, P. Corkum, F. Ilkov, and P. Dietrich, Phys. Rev. A **54**, 1541 (1996).
[29] T. Zuo and A. D. Bandrauk, Phys. Rev. A **52**, R2511 (1995).
[30] D. M. Villeneuve, M. Y. Ivanov, and P. B. Corkum, Phys. Rev. A **54**, 736 (1996).
[31] L. V. Keldysh, Sov. Phys. JETP **20**, 1307 (1965).
[32] T. Seideman, M. Y. Ivanov, and P. B. Corkum, Phys. Rev. Lett. **75**, 2819 (1995).
[33] S. M. Hankin, D. M. Villeneuve, P. B. Corkum, and D. M. Rayner, Phys. Rev. Lett. **84**, 5082 (2000).
[34] *Conical Intersections: Electronic Structure, Dynamics & Spectroscopy*, Advanced Series in Physical Chemistry, edited by W. Domcke, D. R. Yarkony, and H. Koppel (World Scientific, Singapore, 2004).
[35] W. Fuß, W. E. Schmid, and S. A. Trushin, J. Chem. Phys. **112**, 8347 (2000).
[36] N. Nakashima, S. Shimizu, T. Yatsuhashi, S. Sakabe, and Y. Izawa, J. Photochem. Photobiol. C **1**, 131 (2000).
[37] S. A. Trushin, W. Fuß, and W. E. Schmid, J. Phys. B **37**, 3987 (2004).